AIMS Materials Science, 10(1): 164–181.
DOI: 10.3934/matersci.2023009
Received: 25 July 2022
Revised: 01 January 2023
Accepted: 12 January 2023
Published: 18 January 2023

http://www.aimspress.com/journal/Materials

Research article

Influence of chlorotrifluoroethylene on crystal structure and polymer dynamics of poly(vinylidenefluoride-co-chlorotrifluoroethylene) antibacterial copolymers

Wisatre Kongcharoensuntorn[1] and Pornpen Atorngitjawat[2,*]

[1] Department of Biology, Faculty of Science, Burapha University, Chonburi 20131, Thailand
[2] Department of Chemistry, Faculty of Science, Burapha University, Chonburi 20131, Thailand

* **Correspondence:** Email: pornpena@go.buu.ac.th; Tel: +66-38-191-293;
Fax: +66-38-393-494.

Abstract: The effect of chlorotrifluoroethylene (CTFE) on dynamic relaxations of poly(vinylidenefluoride-co-chlorotrifluoroethylene) films (P(VDF-CTFE)) containing 0, 10, 15 and 20% of CTFE was investigated via broadband dielectric spectroscopy (DRS) and dynamic mechanical analysis (DMA). The interpretation was accompanied by the crystal structure obtained from Fourier transform infrared spectroscopy, wide-angle X-ray diffraction, small-angle X-ray scattering and differential scanning calorimetry. Increment of CTFE contents caused reducing the degree of crystallinity but did not impact the long period, lamellar thickness, and amorphous layer thickness. Four dynamic processes were clearly observed in DRS spectra for the neat poly(vinylidene fluoride) and P(VDF-CTFE) which were attributed to the local motion of amorphous chains (β), the segmental relaxation of amorphous chains (α_1), the local conformational rearrangement of the TGTG′ conformation (α_2) and the process associated with Maxwell–Wagner–Sillars interfacial polarization (α_{MWS}). The extra relaxation was observed for P(VDF-CTFE), which was more likely associated to the molecular motion of CTFE chain segments (α_c), correspondent with DMA results. These PVDF and P(VDF-CTFE) conducted as self-antibacterial materials.

Keywords: fluoropolymer; smart polymer; dielectric relaxation; conformational disorder; lamellar thickness; antibacterial activity

1. Introduction

Poly(vinylidene fluoride) (PVDF) and its copolymers are smart polymers and well known as ferroelectric materials. They are potential for the energy storage capacitors [1–4]. These polymers have a high dielectric constant, high dielectric breakdown strength and high electrical energy density (>20 J/cm^3) [5]. To reduce the cooperative ferroelectricity in the PVDF crystals, various amounts of comonomers such as chlorotrifluoroethylene (CTFE), hexafluoropropylene (HFP) and trifluoroethylene (TrFE) are added at the beginning of the polymerization and randomly incorporated in PVDF [4–8]. It has been reported that both poly(vinylidene fluoride-co-chlorotrifluoroethylene) (P(VDF-CTFE)) and poly(vinylidene fluoride-co-hexafluoropropylene) (P(VDF-HFP)) provide a high energy density of ~25 J/cm^3 and break down field >600 MV/m [5,6], which achieved by reducing a crystalline size of the α-phase [9]. P(VDF-CTFE) shows a dramatic increase of the energy density with the electric field without saturation until reaching the breakdown field, which is different from a neat PVDF [10]. P(VDF-CTFE) random copolymers may have semicrystalline or amorphous structure dependent on CTFE contents. P(VDF-CTFE) containing a small amount of CTFE displays a hexagonal or monoclinic crystalline structure and becomes amorphous when CTFE is higher than 30% [11]. According to the beneficial property of P(VDF-CTFE), the main objective of this work is to investigate the effect of CTFE contents on dynamic relaxations of P(VDF-CTFE) copolymers as a function of temperature and frequency. This investigation would help to understand crystal structure and property relationships of these smart polymers. In addition, other than chemical, physical and ferroelectric properties of fluoropolymers, the antibacterial property has been previously found in polymers containing fluorine such as poly(ethylene terephthalate) coated with 2,3,5,6-tetrafluoro-p-phenylenedimethanol and polytetrafluoroethylene [12,13]. This is due to fluorine atoms in fluoropolymers hindering the bacterial adhesion. However, there are a few investigations of antibacterial activity of commercial fluoropolymers have been reported. Therefore, in this research, a self–antibacterial property of P(VDF-CTFE) films, containing both fluorine and chlorine atoms was preliminarily studied, compared to neat PVDF. This preliminary result would further help to elucidate about the novel antibacterial polymers in nature.

In this current paper, the crystal structure and thermal property of PVDF and P(VDF-CTFE) were examined using Fourier transform infrared spectroscopy (FTIR), wide-angle X-ray diffraction (WAXD), small-angle X-ray scattering (SAXS) and differential scanning calorimetry (DSC). The dynamic relaxations were investigated using dynamic mechanical analysis (DMA) and broadband dielectric relaxation spectroscopy (DRS). These findings set the stage for understanding the crystal structure, properties, and dynamic behaviors of antibacterial PVDF containing CTFE.

2. Materials and methods

2.1. Materials

Solef® 1008 PVDF and Solef® 31008, 31508 and 32008 P(VDF-CTFE) copolymers were obtained and prepared in blown films. The blown films were produced by Brabender single screw extruder with extrusion and die temperature of 250 °C. P(VDF-CTFE) 31008, 31508 and 32008 blown films containing 10, 15, and 20% of CTFE are referred to as PCTFE10, PCTFE15 and PCTFE20, respectively.

2.2. Antibacterial activity test

To verify the effect of CTFE on antibacterial property of PVDF and P(VDF-CTFE) films, the antibacterial activity test was performed. Briefly *Escherichia coli* (*E.coli*) and *Staphylococcus aureus* (*S. aureus*) bacteria were cultured in Nutrient agar. Then 3–5 colonies were suspended into Mueller Hinton Broth (MHB) and incubated at 37 ℃ for 3 h. Each culture was diluted with phosphate buffer solution to 1.5×10^8 colony forming unit per milliliter (CFU/mL). An amount of 100 μL of diluted suspension was transferred to 3 mL of MHB. Each sterile disc (6 mm in diameter) was transferred to the prepared *E. coli* and *S. aureus* suspension. After incubation at 37 ℃ for 24 h, the bacterial suspension was serially diluted with phosphate buffer solution. The bacteria in the diluted suspension were counted by a spread plate method. All tests were analyzed in triplicate. The effectiveness of the antibacterial activity (EAA) was calculated according to Eq 1 [14]:

$$\mathrm{EAA}(\%) = \frac{N_0 - N_S}{N_0} \times 100 \quad (1)$$

where N_0 and N_S refer to the number of CFU/mL for blank (MHB) and the sample respectively.

2.3. Sample characterization

2.3.1. Crystal structure and thermal property

Attenuated total reflectance-Fourier transform Infrared (ATR-FTIR) spectra were acquired using a Thermo Scientific Nicolet 6700 spectrometer, signal averaging 200 scans at a resolution of 2 cm^{-1}.

Wide-angle X-ray diffraction (WAXD) patterns were collected on a Rigaku DMAX/rapid micro diffractometer in transmission mode using a copper point focused source (λ = 0.154 nm) at 50 kV and 40 mA.

Degree of crystallinity and thermal characteristics of PVDF and P(VDF-CTFE) films were performed with a Seiko differential scanning calorimetry (DSC) in the temperature range from −90 to 200 ℃, at a heating rate of 10 ℃/min.

Small-angle X-ray Scattering (SAXS) profiles were collected on a Rigaku SAXS instrument with a CuK_α radiation source (λ = 0.154 nm) and a two-dimensional multi-wire detector with the sample-to-detector distance of 1.5 m. The diameter of the incident X-ray beam at the sample position is approximately 0.8 mm. The diameter of the sensitive area of the detector is 120 mm. Absolute scattering intensities were calculated by comparing the spectra of samples to that of a precalibrated polyethylene (S-2907) secondary standard. Data were azimuthally averaged to yield a one-dimensional profile of the absolute intensity *I(q)* versus scattering vector q ($q = (4\pi/\lambda)\sin\theta$, where 2θ is the scattering angle). Lorentz-corrected SAXS intensity (Iq^2) versus q will be plotted to gain the details of crystalline microstructures. The one-dimensional correlation function *K(r)* versus the correlation distance *r* will calculated based on Eq 2 [15]:

$$K(r) = \frac{1}{2\pi^2}\int_0^\infty q^2 I(q)\cos(qr)\,dq \quad (2)$$

The lamellar thickness, amorphous layer thickness and the linear degree of crystallinity in the

lamellar stack were determined from the one-dimensional correlation function base on the first intercept of *K(r)* with the abscissa *B* and the long period L_p ($L_p = B/x_c x_a$, where x_c, x_a are the crystalline and amorphous volume fraction). The L_p obtained from the first maximum of the one-dimensional correlation function.

2.3.2. Dynamic properties

Dynamic mechanical properties were determined in the tension mode using a TA-Q800 dynamic mechanical analysis (DMA), at frequency of 1 Hz and a heating rate of 5 ^{o}C/min. The storage (*E′*) and loss moduli (*E″*) were determined as a function of the temperatures range from −70 to 160 ℃. The rectangular films of 17 × 6.5 mm and 0.03–0.09 mm thick were used.

Broadband dielectric relaxation spectroscopy (DRS) measurements were performed on a Novocontrol GmbH Concept 40 broadband dielectric spectrometer in the frequency domain range from 0.01 Hz–1 MHz in the temperature range from −100 to 160 ℃. Temperature stability was controlled within ±0.2 ℃. Sample films were sandwiched between brass electrodes of 10 mm in diameter.

3. Results and discussion

3.1. Antibacterial activity test

The verified antibacterial property of PVDF and P(VDF-CTFE) is provided in Table 1. The antibacterial efficiency of MHB (blank), PVDF and P(VDF-CTFE) copolymers against *E. coli* and *S. aureus* was reported as the effectiveness of the antibacterial activity (% EAA) and the average number of survival bacteria colonies (CFU/mL). PVDF and all P(VDF-CTFE) displayed the antibacterial efficiency against both *E. coli* and *S. aureus* and the effectiveness increases with increasing CTFE contents. P(VDF-CTFE) samples designated the better effectiveness against *S. aureus* than *E. coli,* compared to neat PVDF. PCTFE20 yielded the antibacterial effectiveness up to 73.01 and 70.21% for *S. aureus* and *E. coli*, respectively. In addition, the findings presented that the EAA of PVDF is higher than 50% for both *S. aureus* and *E. coli*. This indicates that PVDF itself has rather a good antibacterial property. The finding also shows that introducing chlorine atoms on polymer chains helps improving the antimicrobial activity. This might be due to chlorine atoms of CTFE enhancing antifouling performances by precluding the protein accumulating on polymer surfaces. The mechanisms how to kill bacteria is still unclear. However, from our preliminary experiments it is more likely that polymers containing fluorine and chlorine atoms act as anti-biofilms and then reject the adhesion of bacteria [12,13,16]. This preliminary investigation indicated that polymers containing both chlorine and fluorine atoms are more efficiency to prevent the adhesion of bacteria on the surface [17] than that having only fluorine atoms.

Table 1. Antibacterial activity of PVDF and P(VDF-CTFE) copolymers.

Sample	*E. coli*		*S. aureus*	
	Log CFU/mL	EAA (%)	Log CFU/mL	EAA (%)
MHB	11.01	blank	11.56	blank
PVDF	5.10	53.68	5.58	51.73
PCTFE10	3.90	64.58	4.00	65.40
PCTFE15	3.67	66.67	3.75	67.73
PCTFE20	3.37	70.21	3.12	73.01

3.2. FTIR characterization

FTIR spectra was used to confirm the state of crystalline phases of PVDF and P(VDF-CTFE). Figure 1 displays the comparative FTIR spectra of PVDF and P(VDF-CTFE) in the region from 550 to 1500 cm^{-1}. All films exhibit strong absorption bands at ~614 and 763 cm^{-1}, which have been assigned to CF_2 bending in the α-phase PVDF. The peaks at ~795 and 854 cm^{-1} correspond to CH_2 in-plane bending. The absorption bands at ~975, 1148, and 1210 cm^{-1} is attributed respectively to the CH_2 out-of-plane bending, CF_2 symmetric stretching, and CF_2 asymmetric stretching. These bands have been found to be the characteristic of the vibration absorption of the TGTG′ conformation, anti-parallel orientation of C–F bonds (nonpolar α-phase) [11,18–21]. P(VDF-CTFE) samples exhibit a small peak at 840 cm^{-1}, which correspond to the vibrational frequencies of an all-trans conformation, two neighboring chains parallel to each other called polar β-phase [22].

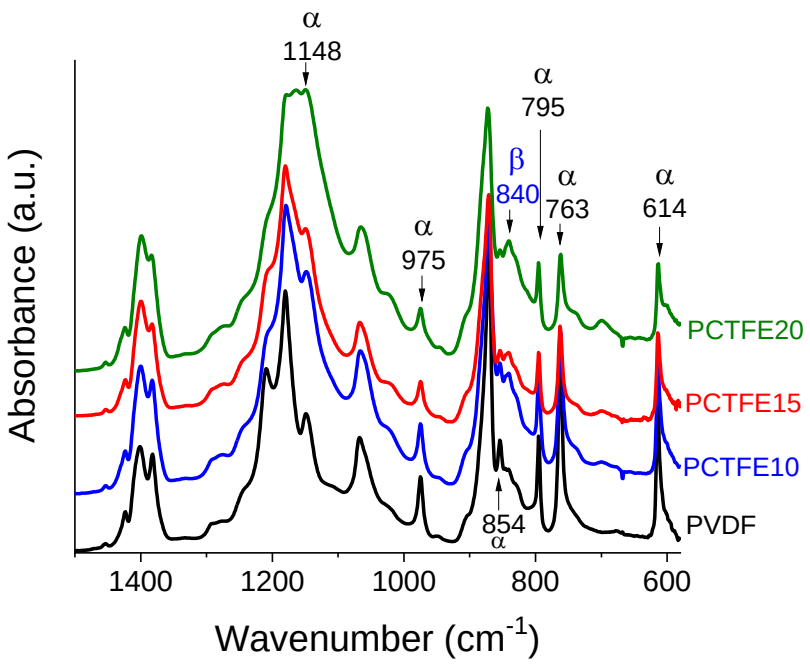

Figure 1. FTIR spectra for PVDF and P(VDF-CTFE) films in the region from 550–1500 cm^{-1}.

3.3. WAXD

Figure 2 displays WAXD pattern of PVDF compared to P(VDF-CTFE) films at 2θ region from 10 ºto 50 º. Owing to the previous investigation [23], the prominent peaks were assigned to the peaks of the α-crystalline phase. Neat PVDF shows the prominent peaks of α (100), α (020), α (110), α (120), α (130) and α (200) [19]. Compared to neat PVDF, P(VDF-CTFE) exhibits three prominent peaks of α (100), α (110) and α (200). The crystal plane of (020), (120) and (130) disappeared for P(VDF-CTFE) due to the CTFE molecules disrupt the molecular chain packing of neat PVDF, which confirms by the degree of crystallinity shown in Table 2. Unlike FTIR results, no β-crystalline phase was observed for P(VDF-CTFE) copolymers. This is probably due to a tiny β-crystalline phase was formed.

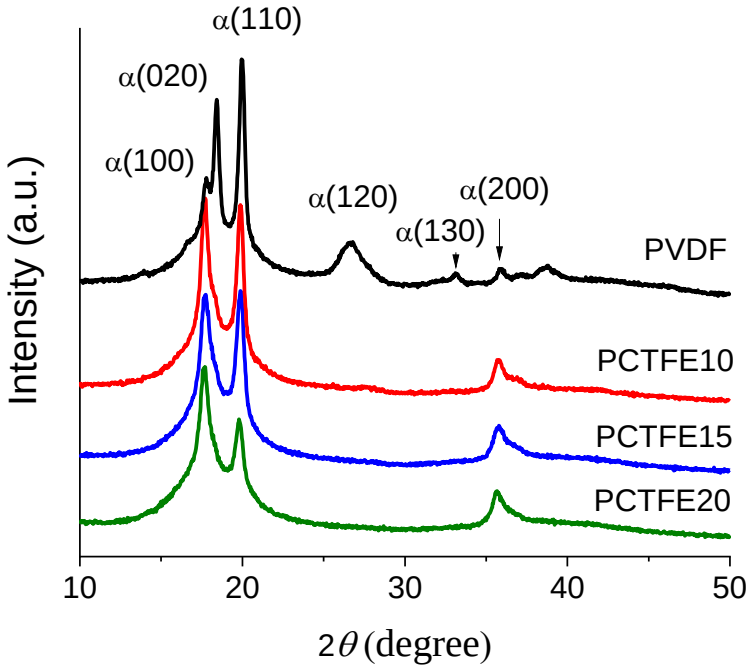

Figure 2. WAXD patterns of PVDF and P(VDF-CTFE) films.

Diffraction peaks were deconvoluted with PeakFit® software by fitting with a Gaussian curve, using a linear baseline. The degree of crystallinity (X_{cw}) was obtained from the fraction of the area under the crystalline peaks to the total area of the amorphous halo and crystalline [24]. As results given in Table 2, the X_{cw} decreases with increasing CTFE contents, which is in good agreement with that observed from DSC technique, illustrating how the bulky CTFE disrupts crystal formation.

Table 2. Degree of crystallinity for PVDF and P(VDF-CTFE) films.

Sample	WAXD	DSC
	X_{cw} (±5%)	X_c (±3%)
PVDF	0.36	0.53
PCTFE10	0.30	0.27
PCTFE15	0.27	0.22
PCTFE20	0.23	0.16

3.4. DSC

As seen in Figure 3a, the melting temperature (T_m), a small endothermic transition (T_{cd}) and glass transition temperature (T_g) are commonly observed for all PVDF and P(VDF-CTFE) samples. Upon cooling, the polymers show sharp exotherms associated with the recrystallization temperature at temperatures lower than T_m (Figure 3b). The inset in Figure 3a displays the glass transition temperature of the samples, which about −37, −36, −26 and −20 ℃, respectively. The transition around 50–60 ℃, denoted as T_{cd}, has been previously assigned to the conformation disorder (T_{cd}) transition in the PVDF crystals [19], which is clearly observed for P(VDF-CTFE) compared to neat PVDF. Although this peak has been assigned to the Curie transition (T_c), ferroelectric-paraelectric transition (TF-P), or the transformation of polar (β, γ, and δ) phases to nonpolar α-phases [15], it is not the case for our investigation. To prove this case, a stretched PVDF film (ST-PVDF), containing almost completely polar β-crystalline phases and an unstretched PVDF film, containing only nonpolar α-crystalline phases (see inset in Figure 3c) were prepared and tested. As seen in Figure 3c, this transition remained the same enthalpy for both stretched and unstretched PVDF films. Therefore, this peak cannot be the transformation of polar to nonpolar phases and the strong transition was observed for all P(VDF-CTFE) copolymers, which contain tiny β-crystalline phases compared to the neat PVDF. In addition, this transition cannot be a Curie temperature, since T_c was previously reported that it relates to mole fractions of VF_2 in PVDF copolymers so T_c of neat PVDF was expected to near 200 ℃ [25]. In addition, T_c of P(VDF-CTFE) should be higher than 50 ℃ and suppose to reduce with increasing CTFE contents. Therefore, from our finding, we proposed that this transition (T_{cd}) is attributed to the conformation disorder in the nonpolar α-crystalline phases.

To confirm the degree of crystallinity obtained from WAXD, the degree of crystallinity was estimated from the enthalpy of T_m peaks (in the temperature range of 100−190 ℃) divided by the ideal melting enthalpy of 100% crystallinity PVDF (=104.5 J/g) [19,26]. Compared with WAXD result, similar trend was observed; the degree of crystallinity (X_c) decreases as the amount of CTFE increases (see Table 2).

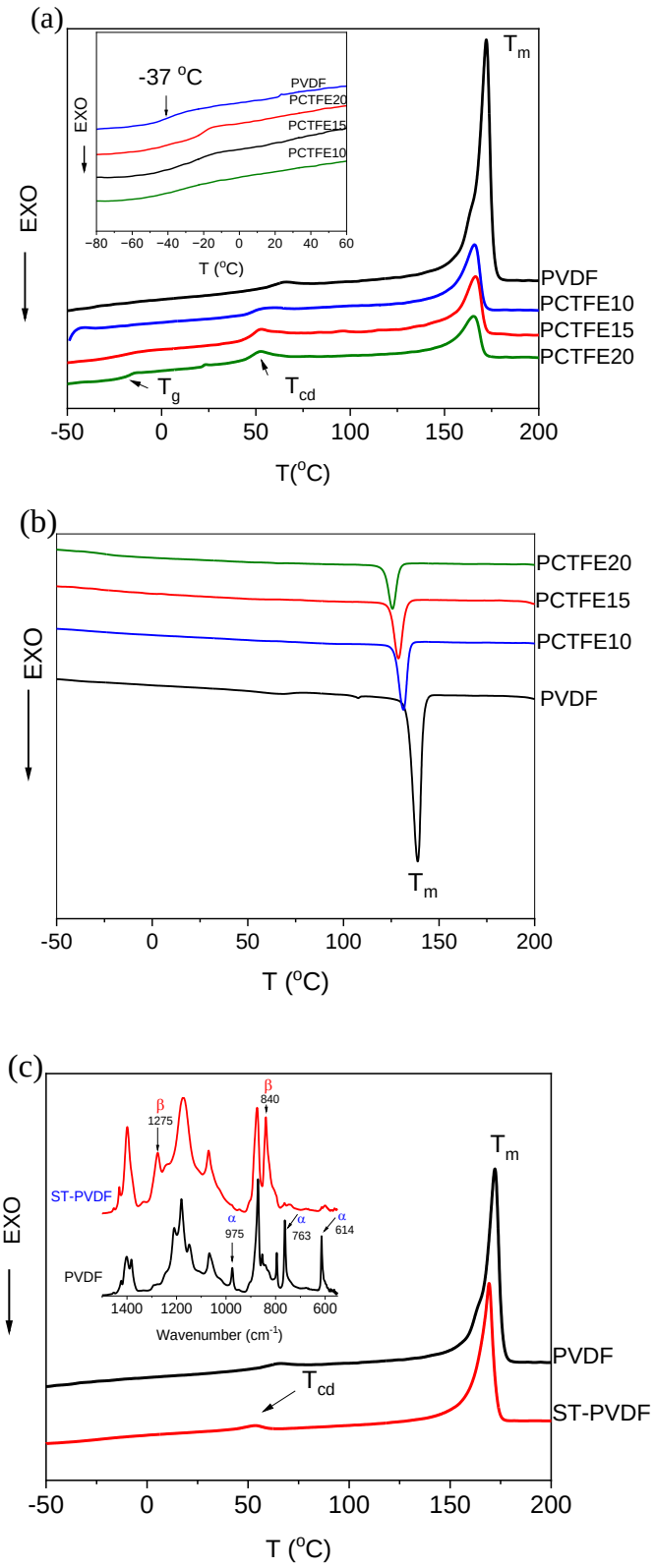

Figure 3. DSC thermograms of (a) PVDF and P(VDF-CTFE) copolymers (heating), (b) PVDF and P(VDF-CTFE) copolymers (cooling) and (c) unstretched (PVDF) and stretched PVDF (ST-PVDF) films. The inset is FTIR spectra of an unstretched (PVDF) and stretched PVDF (ST-PVDF) films.

3.5. SAXS

Figure 4 shows the Lorentz-corrected SAXS intensity (Iq^2) vs. q and the one-dimensional correlation function for PVDF and P(VDF-CTFE) samples. As seen in Figure 4, there is no significant difference between P(VDF-CTFE) and PVDF films. The long period (L_p), lamellar thickness ($l_c = x_c L_p$), amorphous layer thickness ($l_a = x_a L_p$) and the linear degree of crystallinity in the lamellar stack ($X_L = l_c/(l_c + l_a)$) were determined, which are about 89, 69, 26 and 0.73 Å, respectively. The findings suggest that the amount of CTFE does not significantly impact on the value of the long period, lamellar thickness, amorphous layer thickness and linear degree of crystallinity of neat PVDF. This verified that for neat PVDF and P(VDF-CTFE) copolymers with different amounts of CTFE 10–20% (PCTFE10, PCTFE15 and PCTFE20), CTFE molecules do not affect the overall shape of copolymers but to an extent alter the internal arrangements of the PVDF chain. As a result, PVDF and P(VDF-CTFE) have very similar SAXS profiles and different WAXD patterns in some 2θ positions.

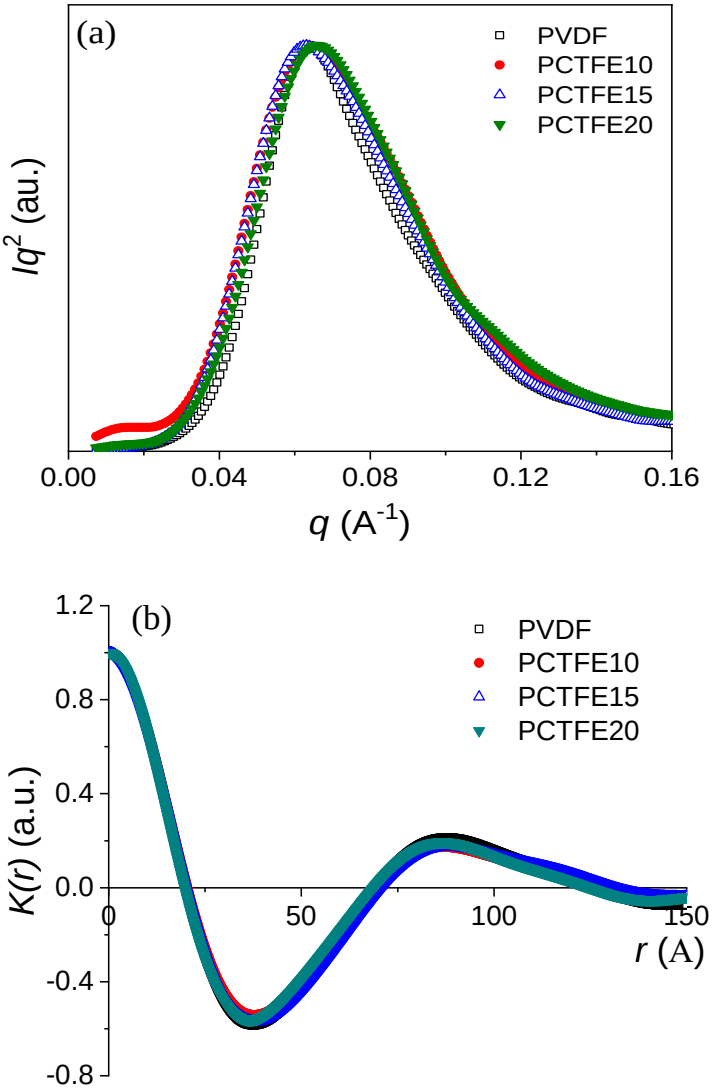

Figure 4. (a) Lorentz-corrected SAXS profiles and (b) one-dimensional correlation function estimated from SAXS patterns for PVDF and P(VDF-CTFE) copolymers.

3.6. DMA

The plots of storage (*E′*) and loss moduli (*E″*) vs. temperatures for PVDF and P(VDF-CTFE) samples are shown in Figure 5. At temperatures above the T_g (about –37 ℃), two relaxations were clearly observed for PVDF (α_1 and α_2) and P(VDF-CTFE) copolymers (α_1 and α_c).

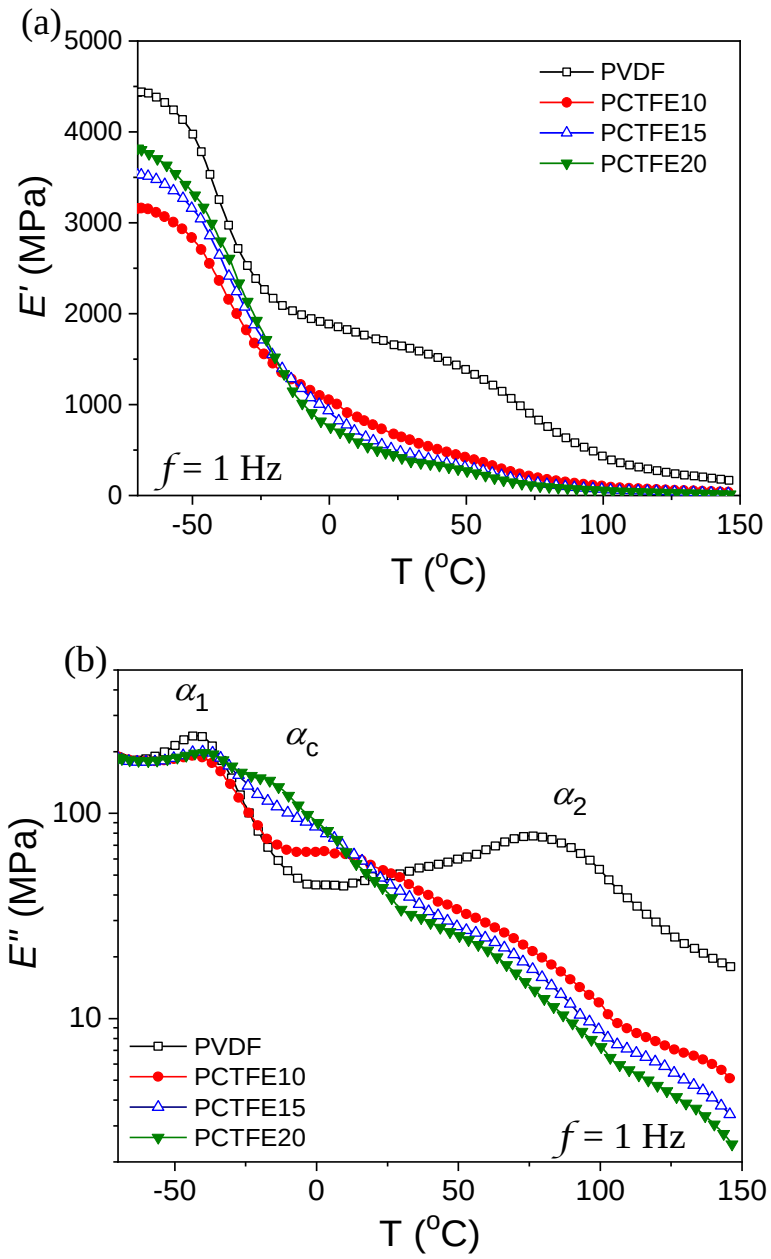

Figure 5. Temperature dependence of (a) storage and (b) loss moduli for PVDF and P(VDF-CTFE) copolymers at 1 Hz.

To clarify the process above T_g, tan δ (tan $\delta = E''/E'$) was plotted as a function of temperatures (Figure 6). Relative to *E″*, three relaxations (α_1, α_c and α_2) can be seen for P(VDF-CTFE) polymers. Previously, the α_1 and α_2 have been assigned to the segmental motion of amorphous chains and the

local conformational rearrangement of the α-crystalline phase, respectively [19]. The α_c transition was only observed for P(VDF-CTFE) copolymers, therefore the α_c transitions are more likely associated to the motions within regions of CTFE [27]. This transition will be further elucidated along with DRS studies. Interestingly the loss magnitude of the α_c was much higher when the CTFE content increased, PCTFE20 > PCTFE15 > PCTFE10. This tendency follows a typical motion of amorphous chain segments, which indicates that amorphous chains are free from crystal restraints. PCTFE20 requires the lowest energy to move because it contains the lowest degree of crystallinity.

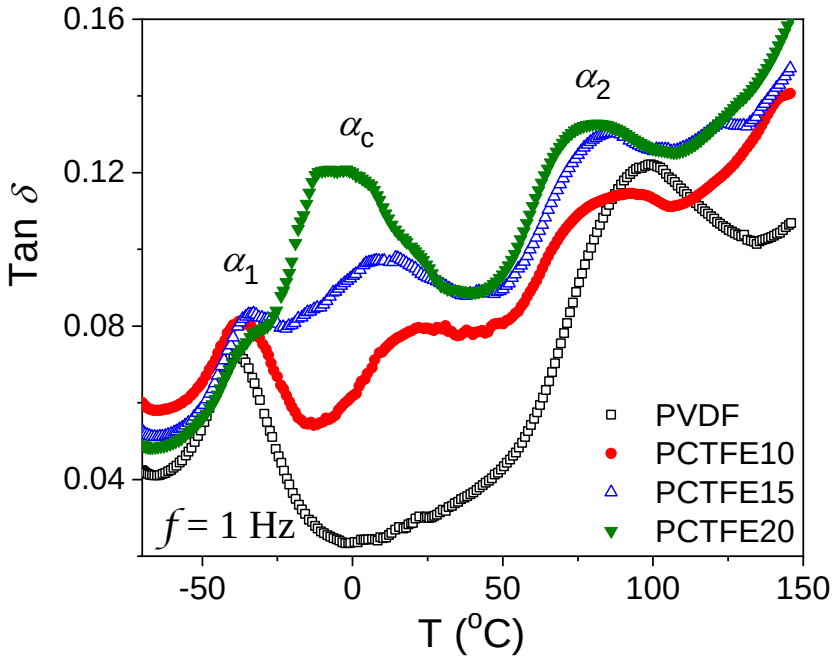

Figure 6. tan δ as a function of temperatures for PVDF and P(VDF-CTFE) copolymers at 1 Hz.

3.7. DRS

The dielectric constant ε' and dielectric loss ε'' were collected from DRS measurement. At high temperature with low frequency, the conduction loss created from the motion of the impurity ions obscures some dipole relaxations. The first derivative of ε' ($\varepsilon''_{der} = -\frac{\pi}{2}\frac{\partial\,\varepsilon'(f)}{\partial\,lnf}$) has been used to elucidate the relaxation of the conduction-free dielectric loss, helpful for identifying a dipole relaxation of materials with high conduction losses. In addition, previously the derivative loss (ε''_{der}) has been shown to partially resolve overlapping relaxations [28]. Figure 7 shows the temperature dependence of ε''_{der} at a frequency of 1 Hz of the neat PVDF and P(VDF-CTFE) copolymers. Four relaxations were clearly observed for PVDF (β, α_1, α_2 and α_{MWS}) and five relaxations were observed for the P(VDF-CTFE) (β, α_1, α_c, α_2 and α_{MWS}). Both PVDF and P(VDF-CTFE) copolymers exhibit the β and α_1 relaxations at the same temperature range below and above T_g, respectively. At temperature above T_g, PVDF exhibits the α_2 relaxation and a Maxwell–Wagner–Sillars (MWS) interfacial polarization (α_{MWS}) between the amorphous and crystalline phases, while the P(VDF-CTFE) displays an extra relaxation, referred to as the α_c relaxation.

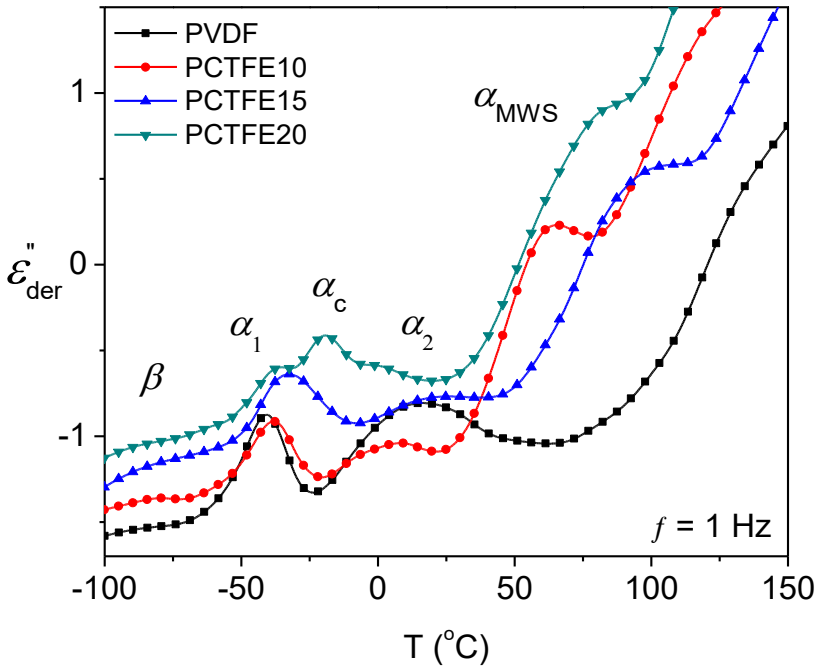

Figure 7. Temperature dependence of ε''_{der} at 1 Hz for PVDF and P(VDF-CTFE) copolymers.

To deep investigation, the dielectric relaxation spectroscopy data processing was performed. The frequency dependence of ε'' at various temperatures was plotted and fit with the appropriate empirical Havriliak-Negami equation as shown in Eq 3 [29]:

$$\varepsilon'' = -\sum_{r=1}^{n} \mathrm{Im} \frac{\Delta\varepsilon_r}{(1+(i\omega\tau_{HNr})^{m_r})^{n_r}} + \frac{\sigma_0}{(\omega\varepsilon_0)^s} \quad (3)$$

The characteristic relaxation time (τ_{HN}) and dielectric relaxation strength ($\Delta\varepsilon$) were obtained by fitting with Eq 3. The frequency maximum was calculated from Eq 4 [30]:

$$f_{max} = \frac{1}{2\pi\tau_{HN}} \left[\frac{\sin\left(\frac{m\pi}{2+2n}\right)}{\sin\left(\frac{mn\pi}{2+2n}\right)}\right]^{1/m} \quad (4)$$

where ω is the angular frequency. m and n are the shape parameters. σ_0 is the dc conductivity (S/cm), ε_0 is the permittivity of free space and the parameter s relates to the type of conduction process.

PVDF and P(VDF-CTFE) copolymers clearly exhibit four strong relaxations, denoted as β, α_1, α_2, and α_{MWS} as temperatures increase. The β relaxations were observed below T_g. This relaxation appeared within a temperature range from −100 to −50 °C. Above −50 °C this relaxation was ceased and taken over by the α_1 relaxation (see Figure 7). The α_2 relaxations were observed from −10 to 160 °C and the α_{MWS} begins to occur at ~100 °C.

The temperature dependence of all relaxations, except α_1 process, follows the Arrhenius law, $f_{max} = f_0\exp[-(E_a/RT)]$ as shown in Figure 8. The α_1 process has the temperature dependence following the Vogel-Fulcher-Tammann (VFT) relation, $f_{max} = f_0\exp[-DT_0/(T-T_0)]$ [31].

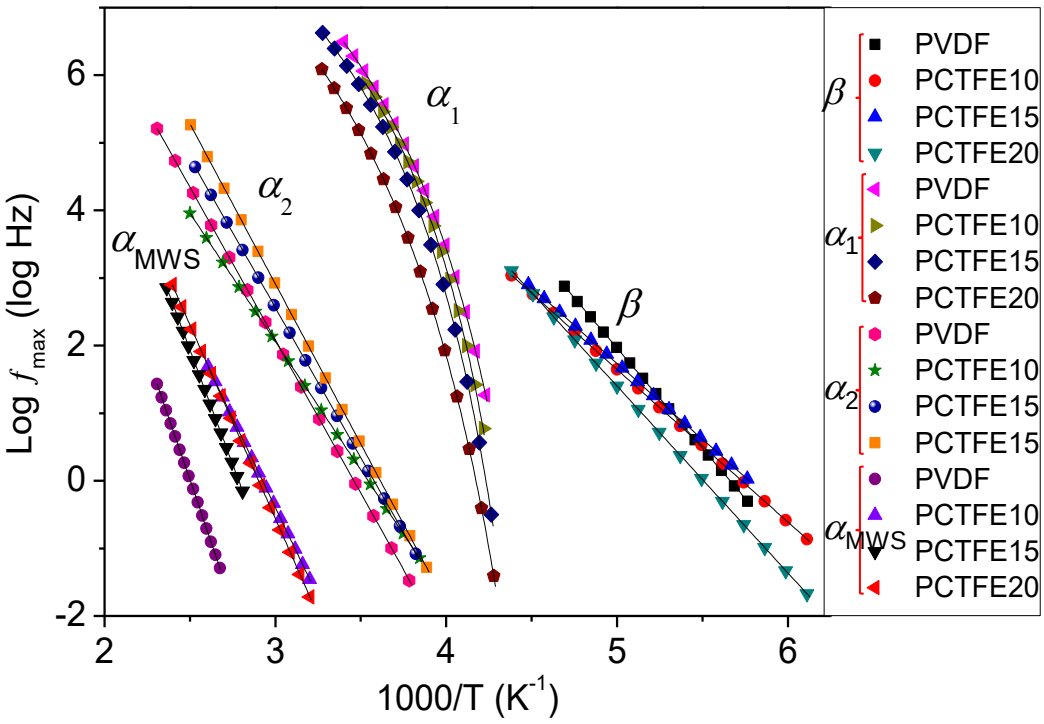

Figure 8. Temperature dependence of the relaxation times for the β, α_1, α_2 and α_{MWS} processes for PVDF and P(VDF-CTFE) copolymers.

Below T_g, the β process exhibits an Arrhenius behavior with the activation energy range of 43–57 kJ/mol as given in Table 3, which is previously assigned to the local relaxation, arising from rotational motions of amorphous chains. The second relaxation appears above T_g but lower than T_{cd}, denoted as the α_1 process, and followed the nonlinear VFT behavior. Therefore, the α_1 relaxation is assigned to the segmental motion of amorphous chains, which agrees well with previous investigations [19]. The α_2 relaxation that is slower than the α_1 process exhibits Arrhenius temperature dependence which represents the typical local relaxation behavior with the activation energy range of 73–91 kJ/mol (see Table 3). Since this relaxation was observed at the temperature below T_{cd} and follows Arrhenius equation, it is more likely related to a local non-cooperative relaxation. Furthermore, as given in Table 4 the $\Delta\varepsilon$ (α_2) is twice higher than the $\Delta\varepsilon$ (β) but less than the $\Delta\varepsilon$ (α_1). According to the evidence from the structure and thermal properties in previous sections and our previous works, this relaxation relates to the local conformational rearrangement of the nonpolar α-crystalline phases of VDF [19]. It has been reported that the conformation disorder could change between TGTG′ and GTG'T conformation [32,33]. In addition, this relaxation was clearly observed although CTFE is incorporated, which has no significant difference of the activation energy with increasing CTFE contents. According to FTIR results, PVDF completely contains the nonpolar α-crystalline phase, while P(VDF-CTFE) contains slightly polar β-crystalline phases. This confirms that the α_2 process involves with only the nonpolar α-crystalline phases.

Table 3. Activation energy of the β, α_2, and α_{MWS} processes and the strength parameter of the α_1 process for PVDF and P(VDF-CTFE) copolymers.

Sample	E_a (β) (kJ/mol)	D (α_1)	E_a (α_2) (kJ/mol)	E_a (α_{MWS}) (kJ/mol)
PVDF	56.8	3.2	86.7	141.8
PCTFE10	43.2	3.8	72.7	101.2
PCTFE15	43.0	4.4	84.9	129.8
PCTFE20	52.9	6.5	90.7	109.7

Table 4. Dielectric relaxation strength of the β, α_1, and α_2 processes at selected temperatures for PVDF and P(VDF-CTFE) copolymers.

Sample	$\Delta\varepsilon$ (β) (T = −80 °C)	$\Delta\varepsilon$ (α_1) (T = 10 °C)	$\Delta\varepsilon$ (α_2) (T = 40 °C)
PVDF	0.5	1.7	0.8
PCTFE10	0.6	2.6	1.6
PCTFE15	0.8	3.6	1.1
PCTFE20	1.3	6.7	2.1

As seen in Figure 7, the α_c process was observed for P(VDF-CTFE) copolymers but absent for neat PVDF, consistent to DMA results. Unfortunately, this process is merging with the α_1 relaxation, and results to the broadening of the α_1 relaxation for PCTFE10 and PCTFE15 but slightly excluded for PCTFE20. However, the α_c process of PCTFE20 merges with the α_1 relaxation when frequency is higher than 100 Hz. From the author's knowledge, this relaxation is first time observed. However, unfortunately we are unable to elucidate more information of this relaxation because this weak relaxation exhibits at the frequency closed to that of the segmental relaxation. Based on DMA results, this relaxation is clearly observed for all P(VDF-CTFE) samples with higher loss modulus magnitudes when CTFE increases. This behavior is more likely reflected to the segmental relaxation [34]. Therefore, we proposed that the α_c process is the molecular motion of CTFE chain segments, which is accompanied by VDF segments.

The α_{MWS} process shows the Arrhenius temperature dependence with the high activation energy (E_a > 100 kJ/mol). Due to a high crystallinity in PVDF and P(VDF-CTFE) copolymers, the moving of free ions from amorphous phases is blocked by the crystalline phases and causes a strong increase in ε' at low frequency and high temperatures. Therefore, the α_{MWS} process was proposed to a manifestation of MWS interfacial polarization, arising in multiphase systems. The sharp increase of ε'' at highest temperatures and low frequency is due to electrode polarization (EP), contributed from the accumulation of mobile ions at an electrode interface [19].

The strength parameter (D) was obtained from the VFT behavior of the α_1 relaxation, which represents the topology of potential energy governing the segmental reconfigurations of polymers, reflecting the nature of bond interactions and the configurational entropy available to the system [19,30]. Typically, D was used to express the fragility of polymers, higher D corresponding to lower fragility and higher the configurational entropy available to the system. As seen in Table 3, the fragility decreases with increasing CTFE contents because of lower degree of crystallinity (see Table 2) and greater entropy of the system. Comparisons of dielectric relaxation strength ($\Delta\varepsilon$) of β, α_1, and α_2

processes, at selected temperatures, are provided in Table 4. The $\Delta\varepsilon$ of β, α_1, and α_2 relaxations increases with rising CTFE content. An increment of $\Delta\varepsilon$ is mainly influenced by an increase of the dipole moment of CTFE structure.

4. Conclusions

Neat PVDF had completely nonpolar α-crystalline phases, while P(VDF-CTFE) copolymers contained slightly polar β-crystalline phases. Three transition temperatures were observed for all samples, which are the glass transition temperature (T_g), the melting temperature (T_m), and the conformation disorder in nonpolar α-crystalline phases (T_{cd}). There were no significant changes on the long period, lamellar thickness, amorphous layer thickness and linear degree of crystallinity when CTFE was copolymerized with VDF up to 20%. The degrees of crystallinity decreased with increasing CTFE contents. At temperatures above T_g, three relaxations (α_1, α_2 and α_c) were clearly observed by DMA for P(VDF-CTFE) copolymers. Four relaxation processes were clearly observed in DRS spectra for the neat PVDF which are attributed to the local motion of amorphous chains (β), the segmental relaxation of amorphous chains (α_1), the local conformational rearrangement of the TGTG′ conformation (α_2) and the process arising from Maxwell–Wagner–Sillars interfacial polarization (α_{MWS}). Other than four relaxations, the extra relaxation was observed for P(VDF-CTFE) copolymers, which was more likely associated to the molecular motion of CTFE chain segments (α_c). P(VDF-CTFE) copolymers are effective on inhibiting viable growth of both *S. aureus* and *E. coli* up to 73.01 and 70.21%, respectively. The antibacterial effectiveness increased with increasing CTFE contents for both *S. aureus* and *E. coli*. Chlorine atoms existing in fluoropolymers enhanced an antibacterial ability.

Acknowledgments

The author would like to special thank Prof. James Runt, The Penn State University, USA for all supports. Authors thanks the Faculty of Science, Burapha University, Thailand.

Conflict of Interest

The authors declare no conflict of interest.

References

1. Bruno A (2009) From vinylidene fluoride (VDF) to the applications of VDF-containing polymers and copolymers: Recent developments and future trends. *Chem Rev* 109: 6632–6686. https://doi.org/10.1021/cr800187m
2. Chu BJ, Zhou X, Ren KL, et al. (2006) A dielectric polymer with high electric energy density and fast discharge speed. *Science* 313: 334–336. https://doi.org/10.1126/science.1127798
3. Tjong SC (2018) Polyvinylidene fluoride: a versatile polymer for biomedical, electronic, energy and environmental applications. *EXPRESS Polym Lett* 12: 395–395. https://doi.org/10.3144/expresspolymlett.2018.33

4. Hamdi O, Mighri F, Denis R (2018) Piezoelectric cellular polymer films: Fabrication, properties and applications. *AIMS Mater Sci* 5: 845–869. https://doi.org/10.3934/MATERSCI.2018.5.845
5. Wang Y, Zhou X, Chen Q, et al. (2010) Recent development of high energy density polymers for dielectric capacitors. *IEEE T Dielect El In* 17: 1036–1042. https://doi.org/10.1109/TDEI.2010.5539672
6. Zhou X, Chu B, Neese B, et al. (2007) Electrical energy density and discharge characteristics of a poly(vinylidene fluoride chlorotrifluoroethylene) copolymer. *IEEE T Dielect El In* 14: 1133–1138. https://doi.org/10.1109/TDEI.2007.4339472
7. Lee JH, Lee B, Won JW, et al. (2017) Synthesis of novel telechelic fluoropolyols based on vinylidene fluoride/hexafluoropropylene copolymers by iodine transfer polymerization. *Macromol Res* 25: 1028–1034. https://doi.org/10.1007/s13233-017-5137-2
8. Ren X, Meng N, Yan H, et al. (2019) Remarkably enhanced polarisability and breakdown strength in PVDF-based interactive polymer blends for advanced energy storage applications. *Polymer* 168: 246–254. https://doi.org/10.1016/j.polymer.2019.02.054
9. Guan F, Pan J, Wang J, et al. (2010) Crystal orientation effect on electric energy storage in poly(vinylidene fluoride-co-hexafluoropropylene) copolymers. *Macromolecules* 43: 384–392. https://doi.org/10.1021/ma901921h
10. Ranjan V, Yu L, Nardelli MB, et al. (2007) Phase equilibria in high energy density PVDF-based polymers. *Phys Rev Lett* 99: 047801. https://doi.org/10.1103/PhysRevLett.99.047801
11. Kalfoglou NK, Williams HL (1973) Mechanical relaxations of poly(vinylidene fluoride) and some of its copolymers. *J Appl Polym Sci* 17: 3367–3373. https://doi.org/10.1002/app.1973.070171111
12. Bao Q, Nishimura N, Kamata H, et al. (2017) Antibacterial and anti-biofilm efficacy of fluoropolymer coating by a 2,3,5,6-tetrafluoro-p-phenylenedimethanol structure. *Colloid Surface B* 151: 363–371. https://doi.org/10.1016/j.colsurfb.2016.12.020
13. Gyo M, Nikaido T, Okada K, et al. (2008) Surface response of fluorine polymer-incorporated resin composites to cariogenic biofilm adherence. *Appl Environ Microbiol* 74: 1428–1435. https://doi.org//10.1128/AEM.02039-07
14. Sedlarik V, Galya T, Sedlarikova J, et al. (2010) The effect of preparation temperature on the mechanical and antibacterial properties of poly(vinyl alcohol)/silver nitrate films. *Polym Degrad Stab* 95: 399–404. https://doi.org/10.1016/j.polymdegradstab.2009.11.017
15. Linares A, Nogales A, Sanz A, et al. (2010) Restricted dynamics in oriented semicrystalline polymers: poly(vinylidene fluoride). *Phys Rev E* 82: 031802. https://doi.org/10.1103/PhysRevE.82.031802
16. Xia WW, Xia MM, Feng X, et al (2018) Surface modification of poly(vinylidene fluoride) ultrafiltration membranes with chitosan for anti-fouling and antibacterial performance. *Macromol Res* 26: 1225–1232. https://doi.org/10.1007/s13233-019-7019-2
17. Popelka A, Novak I, Lehocky M, et al. (2015) Antibacterial treatment of LDPE with halogen derivatives via cold plasma. *Express Polym Lett* 9: 402–411. https://doi.org/10.3144/expresspolymlett.2015.39
18. Nakhmanson SM, Korlacki R, Johnston JT, et al. (2010) Vibrational properties of ferroelectric β-vinylidene fluoride polymers and oligomers. *Phys Rev B* 81: 174120. https://doi.org/10.1103/PhysRevB.81.174120

19. Atorngitjawat P (2017) Effects of processing conditions and crystallization on dynamic relaxations in semicrystalline poly(vinylidene fluoride) films. *Macromol Res* 25: 391–399. https://doi.org/ 10.1007/s13233-017-5060-6
20. Bargainab F, Thuauc D, Panined P, et al. (2019) Thermal behavior of poly(VDF-ter-TrFE-ter-CTFE) copolymers: Influence of CTFE termonomer on the crystal-crystal transitions. *Polymer* 161: 64–77. https://doi.org/10.1016/j.polymer.2018.11.064
21. Barrau S, Ferri A, Costa AD (2018) Nanoscale investigations of α- and γ crystal phases in PVDF-based nanocomposites. *ACS Appl Mater Interfaces* 10: 13092−13099. https://doi.org/10.1021/acsami.8b02172
22. Buonomenna MG, Macchi P, Davoli M, et al. (2007) Poly(vinylidene fluoride) membranes by phase inversion: the role the casting and coagulation conditions play in their morphology, crystalline structure and properties. *Eur Polym J* 43: 1557–1572. https://doi.org/10.1016/j.eurpolymj.2006.12.033
23. Naegele D, Yoon DY, Broadhurst MG (1978) Formation of a new crystal form (α_p) of poly(viny1idene fluoride) under electric field. *Macromolecules* 11: 1297–1298. https://doi.org/10.1021/ma60066a051
24. Dai R, Huang M, Ma L, et al. (2020) Study on crystal structure and phase transitions of polyamide 12 via wide-angle X-ray diffraction with variable temperature. *Adv Compos Hybrid Ma* 3: 522–529. https://doi.org/10.1007/s42114-020-00192-y
25. Thomas DG (1988) Structure, morphology and models of polymer ferroelectrics, In: Wang TT, Herbert JM, Glass AM, *The Applications of Ferroelectric Polymers*, Glasgow: Blackie, 53. https://doi.org/10.1002/actp.1989.010400310
26. Sharma M, Quamara JK, Gaur A (2018) Behaviour of multiphase PVDF in (1–x)PVDF/(x)$BaTiO_3$ nanocomposite films: structural, optical, dielectric and ferroelectric properties. *J Mater Sci Mater Electron* 29: 10875–10884. https://doi.org/10.1007/s10854-018-9163-4
27. Li H, Tan K, Hao Z, et al. (2011) Thermal characterization of a series of poly(vinylidenefluoride-chlorotrifluoroethylene-trifluoroethylene) terpolymer films. *J Therm Anal Calorim* 105: 357–364. https://doi.org/ 10.1007/s10973-011-1427-7
28. Atorngitjawat P, Pipatpanyanugoon K, Aree T (2014) Structure and dielectric relaxations of antibacterial sulfonated polystyrene and silver nanocomposites. *Polym Adv Technol* 25: 1027–1033. https://doi.org/10.1002/pat.3347
29. Wubbenhorst M, van Turnhout J (2002) Analysis of complex dielectric spectra I: one-dimensional derivative techniques and three-dimensional modelling. *J Non-Cryst Solids* 305: 40–49. https://doi.org/ 10.1016/S0022-3093(02)01086-4
30. Masser KA, Runt J (2010) Dynamics of polymer blends of a strongly inter-associating homopolymer with poly(vinyl methyl ether) and poly(2-vinyl pyridine). *Macromolecules* 43: 6414–6421. https://doi.org/10.1021/ma1011396
31. Frenzel F, Borchert P, Anton AM, et al. (2019) Charge transport and glassy dynamics in polymeric ionic liquids as reflected by their inter- and intramolecular interactions. *Soft Matter* 15: 1605–1618. https://doi.org/10.1039/c8sm02135j
32. Yasuhiro T, Hiroyuki T (1980) Formation mechanism of Kink bands in modification II of poly(vinylidene fluoride): evidence for flip-flop motion between $TGTG^-$ and TG^-TG conformations. *Macromolecules* 13: 1316–1317. https://doi.org/10.1021/ma60077a056

33. Morton RE, Balik CM (1990) Modeling of the epitaxial crystallization of poly(vinylidene fluoride): T_2, TGTG′ and T_3GT_3G' chain conformations on (111) calcium fluoride. *Macromolecules* 23: 680–682. https://doi.org/10.1021/ma00204a051
34. Murayama T (1978) *Dynamic Mechanical Analysis of Polymeric material*, New York: Elsevier Scientific Publishing Company, 60–65.

AIMS Press